

# Cross sections of proton-induced nuclear reactions on bismuth and lead up to 100 MeV

L. Mokhtari Oranj,<sup>1</sup> N. S. Jung,<sup>2</sup> M. Bakhtiari,<sup>2</sup> A. Lee,<sup>2</sup> and H. S. Lee<sup>2,\*</sup>

<sup>1</sup>*Division of Advanced Nuclear Engineering, POSTECH, Pohang 37673, Republic of Korea*

<sup>2</sup>*Pohang Accelerator Laboratory, POSTECH, Pohang 37673, Republic of Korea*

(Received 1 November 2016; revised manuscript received 19 February 2017; published 18 April 2017)

Production cross sections of  $^{209}\text{Bi}(p, xn)^{207,206,205,204,203}\text{Po}$ ,  $^{209}\text{Bi}(p, pxn)^{207,206,205,204,203,202}\text{Bi}$ , and  $^{\text{nat}}\text{Pb}(p, xn)^{206,205,204,203,202,201}\text{Bi}$  reactions were measured to fill the gap in the excitation functions up to 100 MeV as well as to figure out the effects of different nuclear properties on proton-induced reactions including heavy nuclei. The targets were arranged in two different stacks consisting of Bi, Pb, Al, Au foils and Pb plates. The proton beam intensity was determined by the activation analysis method using  $^{27}\text{Al}(p, 3pn)^{24}\text{Na}$ ,  $^{197}\text{Au}(p, pn)^{196}\text{Au}$ , and  $^{197}\text{Au}(p, p3n)^{194}\text{Au}$  monitor reactions in parallel as well as the Gafchromic film dosimetry method. The activities of produced radionuclei in the foils were measured by the HPGe spectroscopy system. Over 40 new cross sections were measured in the investigated energy range. A satisfactory agreement was observed between the present experimental data and the previously published data. Excitation functions of mentioned reactions were calculated by using the theoretical model based on the latest version of the TALYS code and compared to the new data as well as with other data in the literature. Additionally, the effects of various combinations of the nuclear input parameters of different level density models, optical model potentials, and  $\gamma$ -ray strength functions were considered. It was concluded that if certain level density models are used, the calculated cross sections could be comparable to the measured data. Furthermore, the effects of optical model potential and  $\gamma$ -ray strength functions were considerably lower than that of nuclear level densities.

DOI: [10.1103/PhysRevC.95.044609](https://doi.org/10.1103/PhysRevC.95.044609)

## I. INTRODUCTION

Natural lead and bismuth are in high demand for shielding applications or widely used in different nuclear technologies as target materials. For this reason, several research groups have studied the cross sections of the reactions on Bi and Pb irradiated with protons [1–16]. However, for the reactions  $^{209}\text{Bi}(p, xn)^{205,204,203}\text{Po}$ ,  $^{209}\text{Bi}(p, pxn)^{207,206,205,204,203,202}\text{Bi}$ , and  $^{\text{nat}}\text{Pb}(p, xn)^{202,201}\text{Bi}$  the experimental data were rare. Therefore, there is a pressing need for conducting experiments and evaluating nuclear data on these nuclear reactions.

In this study, production cross sections of proton-induced nuclear reactions on  $^{209}\text{Bi}$  and  $^{\text{nat}}\text{Pb}$  were measured from 62 to 100 MeV by using the stacked-foil activation technique. Additionally, excitation functions of the reactions were calculated by using the theoretical model calculations based on the code TALYS-1.8 [17]. In our recent works [18,19], the effects of different optical model parameters and phenomenological level density models on some nuclear reactions were presented. In this work, the effects of different nuclear properties on the nuclear reactions, i.e., different nuclear level density (NLD) models, optical model potentials (OMPs), and  $\gamma$ -ray strength functions ( $\gamma$ SFs), were considered with all 768 possible combinations to find out the variation of the theoretical cross sections due to the lack of knowledge of nuclear properties.

This work aimed to extend the nuclear database to the heavy target elements related to proton-induced reactions and accelerator-based technologies to provide a reliable database for theoretical and experimental purposes. We report the measured cross sections of the  $^{209}\text{Bi}(p, xn)^{207,206,205,204,203}\text{Po}$ ,

$^{209}\text{Bi}(p, pxn)^{207,206,205,204,203,202}\text{Bi}$  and  $^{\text{nat}}\text{Pb}(p, xn)$

## II. METHODS

### A. Target preparation

In this paper, results of two irradiation experiments, using Bi and Pb activation foils, are reported. The irradiation experiments were carried out at the high-intensity proton linac facility (KOMAC) in Korea. The Bi and Pb activation foils were arranged in two different stacks. Schematic views of targets are illustrated in Figs. 1(a) and 1(b). Bi activation foils were placed between two Al foils to avoid cross contamination and recoil effects. For the investigation of proton-induced reactions on Bi, the target was arranged in a stack consisting of one Au ( $19.3 \text{ g cm}^{-3}$ , 99.95% purity), twelve Au ( $2.69 \text{ g cm}^{-3}$ , 99.999% purity), and five Bi ( $9.8 \text{ g cm}^{-3}$ , 99.97% purity) foils together with four 2-mm-thick and one 9-mm-thick Pb plates. The typical thickness of individual Au, Al, and Bi foils was 30, 100, and 50  $\mu\text{m}$ , respectively. To study proton-induced reactions on Pb, a target was arranged in a stack consisting of one Au, nine Al, and nine Pb ( $11.35 \text{ g cm}^{-3}$ , 99.99+ % purity) foils together with three 5-mm-thick Pb plates. The typical thickness of individual Au, Al, and Pb foils was 30, 100, and 125  $\mu\text{m}$ , respectively. Similar to the Bi activation foils discussed above, Pb activation foils were placed between two Pb foils to avoid cross contamination and recoil effects. Consequently, only the inner Pb foils were used for radionuclei measurements. In addition to the activation foils, Al monitor foils were also placed between two Al foils. The cross-sectional size of the targets was about  $5 \text{ cm} \times 5 \text{ cm}$ . Natural Pb plates were placed between Bi and Pb activation foils to degrade proton beam energy.

\*Corresponding author: lee@postech.ac.kr

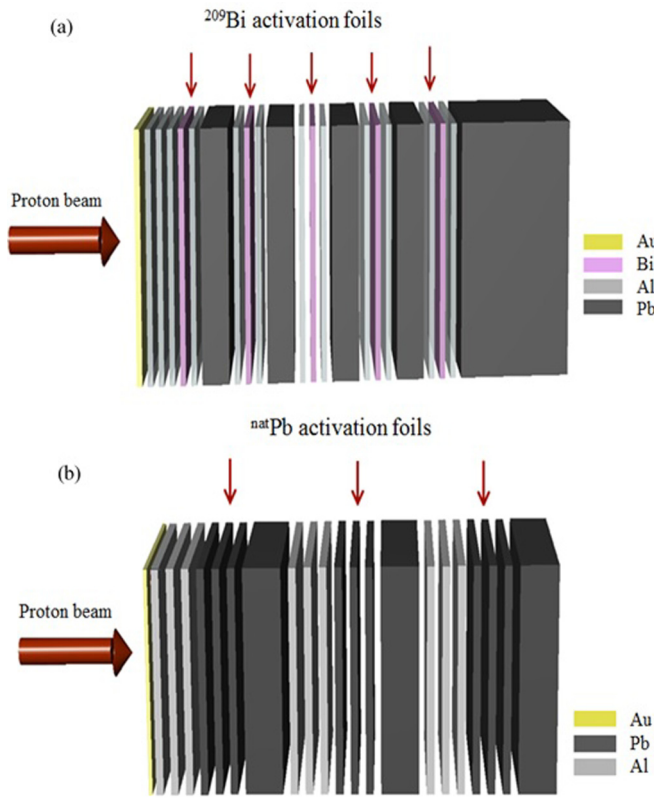


FIG. 1. Schematic view of the (a) Bi and (b) Pb targets.

The total thickness of irradiated targets for the bismuth and lead foils was designed to be 1.8 and 1.6 cm, respectively, which is larger than the range of 100-MeV protons in the targets, 1.4 cm, calculated by SRIM-2010 [20].

In addition, a vacuum window composed of  $\text{Al}_4\text{Be}_6$  (500  $\mu\text{m}$  thickness,  $2.1 \text{ g cm}^{-3}$ ) was placed at the end of the proton beam vacuum pipe at 1.7 m from the target. The Au and Al foils were placed at the beginning of the target stack to determine the proton beam intensity. Also, a Gafchromic film with dimensions of  $7 \text{ cm} \times 7 \text{ cm}$  was used to measure the beam intensity and two-dimensional beam profile.

### B. $\gamma$ spectrum analysis and determination of cross sections

After each irradiation, the  $\gamma$ -ray spectra of activation foils were measured using HPGe detectors with a relative efficiency of 15 or 20% at 5 and 21.5 cm from the surface of detector for Pb and Bi, respectively. The shortest cooling time was set up to be about half an hour to measure the production yields of short-lived radionuclides. The efficiency of the HPGe detector was experimentally determined using standard multiple  $\gamma$ -ray sources,  $^{152}\text{Eu}$ ,  $^{137}\text{Cs}$ , and  $^{133}\text{Ba}$  at 5 and 21.5 cm from the surface of the detector for Pb and Bi, respectively. The spectrum analysis was done by the Canberra's Genie-2000 gamma analysis software package (version 3.2) [21].

The activities of the Bi and Pb activation foils and monitor foils were measured for a counting time of  $t_C = t_{\text{EoC}} - t_{\text{BoC}}$ , starting from the time at the beginning of counting ( $t_{\text{BoC}}$ ) to the time at the end of counting ( $t_{\text{EoC}}$ ). The net area  $N_p(E_\gamma, t_C, t_{\text{BoC}})$

of a full energy peak related to a  $\gamma$ -ray transition of a nuclide with energy  $E_\gamma$  is given by Eq. (1) [11]:

$$N_p(E_\gamma, t_C, t_{\text{BoC}}) = \int_{t_{\text{BoC}}}^{t_{\text{EoC}}} A(t) \varepsilon(E_\gamma) I_\gamma(E_\gamma) dt, \quad (1)$$

where  $\varepsilon(E_\gamma)$  and  $I_\gamma(E_\gamma)$  are the efficiency of detector and absolute branching ratio for the  $\gamma$ -ray energy  $E_\gamma$ , respectively. Integration of Eq. (1) yields the activity at the end of irradiation (EoI):

$$A(t_{\text{EoI}}) = \frac{N_p \lambda}{\varepsilon(E_\gamma) I_\gamma(E_\gamma) [1 - \exp(-\lambda t_c)]} \exp(\lambda t_d) \quad (2)$$

with  $t_d = t_{\text{BoC}} - t_{\text{EoI}}$ , the cooling time between end of irradiation (EoI) and beginning of counting (BoC), and  $\lambda$  the decay constant of the nuclide with half-life of  $T_{1/2}$ .

The variation of activity of the nuclide during the time of irradiation  $t_{\text{irr}}$  of a sample consisting of  $N_T$  target atoms, with projectiles of flux density  $\Phi(\text{cm}^{-2} \text{s}^{-1})$ , is described by Eq. (3):

$$A(t) = N_T \sigma \Phi [1 - \exp(-\lambda t_{\text{irr}})]. \quad (3)$$

Finally, the cross section  $\sigma$  is obtained by combining Eqs. (2) and (3):

$$\sigma = \frac{N_p \lambda}{\Phi N_T \varepsilon(E_\gamma) I_\gamma(E_\gamma)} \frac{\exp(\lambda t_d)}{[1 - \exp(-\lambda t_c)][1 - \exp(-\lambda t_{\text{irr}})]}. \quad (4)$$

Equation (4) calculates an independent cross section if no precursors contribute to the formation of the investigated radionuclide. If a radionuclide is produced through a nuclear reaction and also from the decay of precursors the measured cross sections are cumulative so that Eq. (4) needs to be corrected. Assume a mother nuclide  $m$  of known activity  $A_m$  which decays with decay constant  $\lambda_m$  into the daughter  $d$  with  $\lambda_d$  for which cumulative activities  $A_d^*$  are calculated according to Eq. (2). In such cases the corrected activity  $A_d$  is calculated according to Eq. (5) and the independent cross section of the daughter is calculated by Eq. (6),

$$A_d(t_{\text{EoI}}) = A_d^*(t_{\text{EoI}}) + A_m(t_{\text{EoI}}) \frac{\lambda_d}{\lambda_d - \lambda_m} \times \left( 1 - \frac{\lambda_d}{\lambda_m} \frac{1 - \exp(-\lambda_m t_c)}{1 - \exp(-\lambda_d t_c)} \times \exp[-(\lambda_m - \lambda_d)t_d] \right), \quad (5)$$

$$\sigma_d = \frac{A_d^*(t_{\text{EoI}})}{N_T \Phi [1 - \exp(-\lambda_d t_{\text{irr}})]} - \sigma_m \times \left[ 1 - \frac{\lambda_d}{\lambda_d - \lambda_m} \left( 1 - \frac{1 - \exp(-\lambda_m t_{\text{irr}})}{1 - \exp(-\lambda_D t_{\text{irr}})} \right) \right]. \quad (6)$$

### C. Determination of beam energy and intensity

The targets including Bi and Pb foils were irradiated for 2 and 3.4 min with 103-MeV protons (1 Hz repetition rate), respectively. The beam shape was described by Gaussian distribution at the targets in both  $x$  and  $y$  coordinates (the  $z$  coordinate is the beam direction) based on the beam profile on the Gafchromic film. The full width at half maximum

TABLE I. Decay characteristics of the beam monitor reactions [16,25].

Nuclide	Half-life	$E_\gamma$ (keV)	$I_\gamma$ (%)	Contributing reactions	$Q$ value (MeV)
$^{196}\text{Au}$	$6.1669 \pm 0.0006\text{ d}$	333.03	$22.9 \pm 0.9$	$^{197}\text{Au}(p, pn)$	−8.07
		355.73	87		
$^{194}\text{Au}$	$38.02 \pm 0.10\text{ h}$	293.548	$10.6 \pm 0.15$	$^{197}\text{Au}(p, p3n)$	−23.29
		328.464	$60.4 \pm 0.8$		
$^{24}\text{Na}$	$14.997 \pm 0.012\text{ h}$	1368.626	$99.9936 \pm 0.0015$	$^{27}\text{Al}(p, 3pn)$	−31.43
		2754.007	$99.855 \pm 0.005$		

(FWHM) of the distribution was 1.9 and 1.8 cm in the  $x$  and  $y$  direction, respectively. The energy of incident proton beam was calibrated to be  $103 \pm 0.13$  MeV using multienergy degrading techniques [22].

The energy distribution of protons onto the front surface of Bi and Pb activation foils was obtained using FLUKA Monte Carlo code [23]. Regarding results of FLUKA, incident protons energies that reached the surface of five Bi activation foils were  $100.5 \pm 0.5$ ,  $91.8 \pm 1.0$ ,  $82 \pm 1.5$ ,  $72 \pm 2$ , and  $62 \pm 2.5$  MeV, respectively. Protons energies onto the front surface of three Pb activation foils were  $100 \pm 1.0$ ,  $76 \pm 2.0$ , and  $45 \pm 3.0$  MeV, respectively.

It should be noted that contribution of secondary neutrons and protons coming from the next foil to the cross section were estimated. The contribution of these neutrons and protons was less than 1% and 0.001%, respectively, which could be negligible.

In each experiment, the proton beam intensity was determined by the activation analysis method using the monitor reactions  $^{27}\text{Al}(p, 3pn)^{24}\text{Na}$ ,  $^{197}\text{Au}(p, pn)^{196}\text{Au}$ , and  $^{197}\text{Au}(p, p3n)^{194}\text{Au}$  and also by Gafchromic film dosimetry method in parallel. Prior to irradiation, beam intensity was measured by a Gafchromic film placed at the same location as the target. The film was scanned at 24 h after exposure. The average dose was measured at the center of the film with an area of  $5\text{ cm} \times 5\text{ cm}$ . Proton flux was calculated by Eq. (7) [24]:

$$D(Gy) = \Phi \frac{dE}{dx} \left( \frac{dt}{\rho} \right), \quad (7)$$

where  $D$  is absorbed dose ( $Gy$ ),  $\Phi$  is proton flux ( $\text{protons cm}^{-2} \text{s}^{-1}$ ),  $\frac{dE}{dx}$  is stopping power ( $\text{keV cm}^{-1}$ ),  $dt$  is irradiation time (sec), and  $\rho$  is density of the film ( $\text{g cm}^{-3}$ ), which was assumed to be equal to that of tissue.

The cross sections for the applied monitor reactions were taken from Refs. [16,25]. The decay data of all the reactions were taken from National Nuclear Data Center (NNDC) [26] which are listed in Tables I and II.

Measured activities of monitor reactions and obtained beam intensities of both experiments are given in Table III. As can be seen from Table III, obtained beam intensities using various monitor reactions are consistent. Additionally, comparison between the results from the activation method and Gafchromic film show a satisfactory agreement. Uncertainty of the beam intensity measurement by the activation analysis was estimated by possible uncertainties of measured activities ( $\sim 2.0\%$ ), used cross-sections ( $\sim 10.0\%$ ), and mass of the

monitor activation foils ( $\sim 0.01\%$ ). The overall uncertainty in the beam intensity measurement was estimated to be approximately 10.2%. In this work, the average value of beam intensities, resulting from monitor reactions, was used in Eqs. (4) and (6) to obtain cross sections of desired radionuclei.

#### D. Nuclear model calculations

The production cross sections of the measured radionuclei were calculated by the nuclear model calculation code TALYS-1.8. The TALYS code simulates the nuclear reactions that involve gammas, neutrons, protons, deuterons, tritons,  $^3\text{He}$ , and  $\alpha$ -particles in the incident energy range from 1 keV to 200 MeV for target nuclides of mass of 12 and heavier [17].

TALYS uses by default the phenomenological OMP parametrizations for neutrons and protons on a nucleus-by-nucleus basis to obtain the transmission coefficients and the reaction cross sections. If the phenomenological potential is not available, TALYS automatically uses a global OMP proposed by Koning and Delaroche [27]. The important default input models and parameters for TALYS calculation are as follows: the model of the Hauser-Feshbach [28] for compound nucleus reactions, coupled-channels calculations are automatically invoked when a coupling scheme is available. Constant temperature model (CTM) [29] at low energies, and the Fermi gas model (FGM) [30] at higher energies are automatically applied as the default level density model.  $\gamma$ -ray transmission coefficients are generated with the Kopecky-Uhl generalized Lorentzian for the  $\gamma$  SF [31]. The pre-equilibrium reactions, which become important for incident energies above almost 10 MeV, are modeled using the two-component exciton model [17]. TALYS calculates the portion of different nuclear reaction mechanisms such as compound, pre-equilibrium, and direct. In this work, the dominance of each mechanism is illustrated.

It is assumed that nuclear reactions are dependent on the NLDs, OMP and  $\gamma$  SF [32–34]. Figure 2 shows the contribution of different mechanisms (compound, pre-equilibrium, and direct) to the total reaction cross section for the  $^{nat}\text{Pb}(p, x)$  reactions calculated by TALYS. It can be seen that compound and pre-equilibrium mechanisms are a major portion of reaction cross sections. On the other hand, Hauser-Feshbach compound nucleus theory is used for calculating the cross section into one of the open channels in the reaction. The Hauser-Feshbach model is dependent on three important ingredients: (a) spin and parity of the target and residual nucleus (information of the ground state of target and residual nuclei is obtained from

TABLE II. Data for the measured radionuclei [26].

Nuclide	Half-life	$E_\gamma$ (keV)	$I_\gamma$ (%)	Contributing reactions	$Q$ value (MeV)
$^{207}\text{Po}$	$5.80 \pm 0.02$ h	405.78	9.7		
		742.72	$28.4 \pm 0.7$	$^{209}\text{Bi}(p, 3n) ^{207}\text{Po} \rightarrow ^{207}\text{Bi}$	−18.04
		911.77	$17.0 \pm 0.4$		
		992.39	$59.2 \pm 1.3$		
$^{206}\text{Po}$	$8.8 \pm 0.1$ d	286.41	$22.9 \pm 0.5$		
		338.44	$18.5 \pm 0.4$		
		522.47	$15.1 \pm 0.4$	$^{209}\text{Bi}(p, 4n) ^{206}\text{Po} \rightarrow ^{206}\text{Bi}$	−25.07
		807.38	$21.8 \pm 0.5$		
		980.23	$6.81 \pm 0.16$		
$^{205}\text{Po}$	$1.74 \pm 0.08$ h	1032.26	$31.7 \pm 0.8$		
		836.8	$19.2 \pm 1.5$		
		849.8	$25.5 \pm 2.0$	$^{209}\text{Bi}(p, 5n) ^{205}\text{Po} \rightarrow ^{205}\text{Bi}$	−33.82
		872.4	37		
		1001.2	$28.8 \pm 2.1$		
$^{204}\text{Po}$	$3.519 \pm 0.012$ h	270.06	$31.9 \pm 1.1$		
		762.52	$13.2 \pm 0.4$	$^{209}\text{Bi}(p, 6n) ^{204}\text{Po} \rightarrow ^{204}\text{Bi}$	−41.05
		883.96	$34.3 \pm 0.8$		
		1016.29	$27.6 \pm 0.7$		
		214.8	$14.3 \pm 1.3$		
$^{203}\text{Po}$	$36.7 \pm 0.5$ min	893.5	$18.7 \pm 1.5$	$^{209}\text{Bi}(p, 7n) ^{203}\text{Po} \rightarrow ^{203}\text{Bi}$	−50.16
		908.6	55		
		1090.9	$19.2 \pm 1.5$		
		569.698	$97.75 \pm 0.03$		
		1063.656	$74.5 \pm 0.3$	$^{209}\text{Bi}(p, p2n)$	−14.35
$^{207}\text{Bi}$	$31.55 \pm 0.04$ yr	183.977	$15.8 \pm 0.3$		
		343.51	$23.5 \pm 0.4$		
		398.00	$10.75 \pm 0.15$		
		497.06	$15.33 \pm 0.21$	$^{209}\text{Bi}(p, p3n)$ $^{206}\text{Pb}(p, n)$	−22.44 −4.54
		516.18	$40.8 \pm 0.6$		
		537.45	$30.5 \pm 0.4$		
		803.10	$99.0 \pm 1.4$		
		881.01	$66.2 \pm 1.0$	$^{207}\text{Pb}(p, 2n)$ $^{208}\text{Pb}(p, 3n)$	−11.28 −18.64
		895.12	$15.67 \pm 0.22$		
		1098.26	$13.51 \pm 0.20$		
$^{205}\text{Bi}$	$15.31 \pm 0.04$ d	703.45	31.1	$^{209}\text{Bi}(p, p4n)$ $^{206}\text{Pb}(p, 2n)$	−29.48 −11.57
		987.66	$16.1 \pm 0.3$		
		1764.30	$32.5 \pm 0.7$		
$^{204}\text{Bi}$	$11.22 \pm 0.10$ h	374.76	$82 \pm 8$	$^{209}\text{Bi}(p, p5n)$ $^{206}\text{Pb}(p, 3n)$	−37.97 −20.06
		899.15	$99 \pm 12$		
		983.98	$59 \pm 6$		
		820.2	$30.0 \pm 2.5$		
$^{203}\text{Bi}$	$11.76 \pm 0.05$ h	825.2	$14.8 \pm 1.2$	$^{209}\text{Bi}(p, p6n)$ $^{206}\text{Pb}(p, 4n)$	−45.16 −27.26
		847.2	$8.6 \pm 0.7$		
		896.9	$13.2 \pm 1.1$		
		422.13	$83.7 \pm 2.5$		
$^{202}\text{Bi}$	$1.71 \pm 0.04$ h	657.49	$60.6 \pm 1.8$	$^{209}\text{Bi}(p, p7n)$ $^{206}\text{Pb}(p, 5n)$	−54.02 −36.11
		960.67	99.283		
		629.1	$26.0 \pm 1.7$		
$^{201\text{g}}\text{Bi}$	$103 \pm 3$ min	786.4	$10.3 \pm 0.7$	$^{209}\text{Bi}(p, p8n)$ $^{206}\text{Pb}(p, 6n)$	−61.41 −43.51
		936.2	$12.2 \pm 12.2$		
		1014.1	$11.6 \pm 0.8$		
		208.0	208.0		

TABLE III. Measured yields of  $^{197}\text{Au}(p, pn)^{196}\text{Au}$ ,  $^{197}\text{Au}(p, p3n)^{194}\text{Au}$ , and  $^{27}\text{Al}(p, 3pn)^{24}\text{Na}$  monitor reactions and measured beam intensities.

Experiment	Method		Irradiation time (min)	Production yield (Bq)	Beam intensity ( $\text{Protons s}^{-1}$ )
Bi	Activation analysis	$^{197}\text{Au}(p, pn)^{196}\text{Au}$	2	$535.8 \pm 1.5$	$(1.5 \pm 0.15) \times 10^{11}$
		$^{197}\text{Au}(p, p3n)^{194}\text{Au}$		$1937.8 \pm 26.2$	$(1.5 \pm 0.16) \times 10^{11}$
		$^{27}\text{Al}(p, 3pn)^{24}\text{Na}$		$1652.3 \pm 28.3$	$(1.7 \pm 0.17) \times 10^{11}$
Pb	Dosimetry	Gafchromic	3.4		$1.6 \times 10^{11}$
		$^{197}\text{Au}(p, pn)^{196}\text{Au}$		$46.1 \pm 0.4$	$(7.4 \pm 0.7) \times 10^9$
		$^{197}\text{Au}(p, p3n)^{194}\text{Au}$		$166.5 \pm 2.5$	$(7.7 \pm 0.7) \times 10^9$
Pb	Activation analysis	$^{27}\text{Al}(p, 3pn)^{24}\text{Na}$	3.4	$275.5 \pm 5.5$	$(8.6 \pm 0.9) \times 10^9$
		Gafchromic			$7.4 \times 10^9$

experimental data or from systematics so that the properties of excited states are taken from tables up to a specific energy, and over that energy the data are calculated through a NLD model); (b) transmission coefficients for outgoing particles which are determined from appropriate OMP, and (c) photon transmission coefficients which are obtained from different  $\gamma$ SFs. Therefore, it is worth considering the impact of the different nuclear models on nuclear reactions. TALYS-1.8 includes several OMPs, NLDs, and  $\gamma$ SFs which are listed in Table IV. In the table, there are two different OMPs for nucleon-nucleus interactions, eight  $\alpha$ OMPs, six NLDs, and eight  $\gamma$ SFs; all models are divided into two groups, namely phenomenological and semimicroscopic, and for all models an acronym is used. For instance, KD stands for OMP proposed by Koning and Delaroche. Hence, KD- $\alpha$ OMP III-GSM-HFBQ refers to the combination of (a) the OMP proposed by Koning and Delaroche, (b)  $\alpha$ OMP proposed in Ref. [37] using the dispersive model, (c) the general superfluid level density model, and (d)  $\gamma$ SF described by Khan *et al.* [47]. In this work, all 768 possible combinations for 24 nuclear input parameters were considered not only to determine the theoretical variation in cross sections, but also to find out the sensitivity of

the cross sections to each nuclear model. In the following sections, the measured data in this work are compared to the available published data as well as to the theoretical calculations.

### III. RESULTS AND DISCUSSION

The absolute values of measured cross sections of the investigated radionuclides are collected in Tables V and VI. The excitation functions of interested reactions are shown in Figs. 3–10 together with the nuclear model calculations and earlier works. In the figures, the shaded areas indicate the variation of the cross sections by using different combinations. Cross sections of  $^{209}\text{Bi}(p, xn)^{207,206,205,204,203}\text{Po}$ ,  $^{nat}\text{Pb}(p, xn)^{206,205,204,203,202,201}\text{Bi}$  were calculated using Eq. (4), while, for the reactions  $^{209}\text{Bi}(p, pxn)^{207,206,205,204,203}\text{Bi}$  Eq. (6) was used to induce the independent cross sections from cumulative ones. It should be mentioned that in the case of the reaction  $^{209}\text{Bi}(p, pxn)^{202}\text{Bi}$  there were no  $\gamma$  rays to measure the precursor nucleus ( $^{202}\text{Po}$ ) activity, therefore, the measured cross sections were cumulative. Uncertainties of the measured cross sections of Po and Bi radionuclides were calculated as the sum in quadrature of the possible individual relative uncertainties, which were between 8.5% and 15.7%.

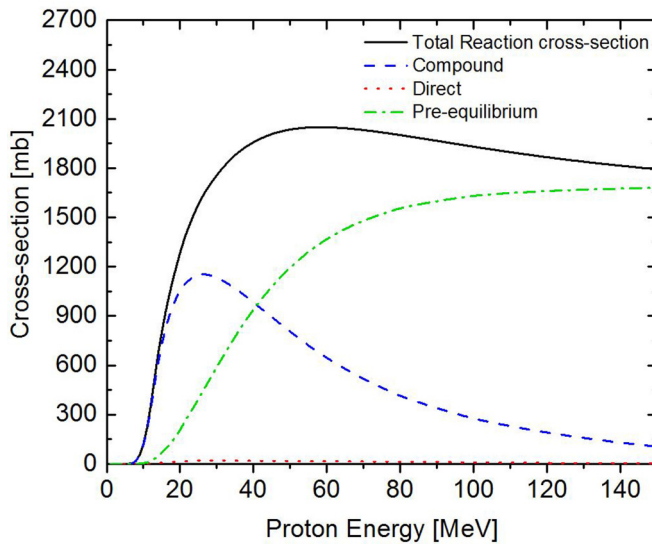


FIG. 2. Contribution of different reaction mechanisms (direct, pre-equilibrium, and compound) to the total reaction cross section calculated by TALYS for  $^{nat}\text{Pb}(p, x)$  processes.

#### A. $^{209}\text{Bi}(p, 3n)^{207}\text{Po}$ and $^{209}\text{Bi}(p, 4n)^{206}\text{Po}$ reactions

Production yields of  $^{207}\text{Po}$  ( $T_{1/2} = 5.80\text{ h}$ ;  $\varepsilon: 99.98\%$ ; and  $\alpha: 0.02\%$ ) were obtained using the 742.72-keV  $\gamma$  ray that was well defined in the spectrum of each irradiated bismuth foil. The measured activities included the contribution of the decay of the simultaneously produced short-lived isomeric state ( $T_{1/2} = 2.79\text{ s}$ ; isomeric transition (IT): 100%) of  $^{207}\text{Po}$ . There were five experimental data sets in the literature for this reaction over different energy ranges within 135 MeV, which was our interest energy range, reported by Chung *et al.* [5], Michel *et al.* [2], Titarenko *et al.* [1], Miyano *et al.* [8], and Belyaev *et al.* [4]. Figure 3(a) shows the comparison of our data with other data. From the figure, the consistency of the data in this work with the data reported by Michel *et al.* [2], Titarenko *et al.* [1], and Belyaev *et al.* [4] is acceptable. In addition, the theoretical calculations with different combinations are shown in Fig. 3(a). The models which are producing the upper and lower borders are indicated in the figures, showing that no single combination always corresponds to upper or lower

TABLE IV. Nuclear input parameters employed to TALYS-1.8. For each model corresponding acronym is shown in the table.

Parameter	Phenomenological	Semimicroscopic
$\alpha$ OMP	1-KD: Global model of Koning and Delaroche [27]	2-Jeukenne-Lejeune-Mahaux by Bauge, Delaroche, and Girod [34]
	1-WKD: Watanabe folding approach [35] with Koning-Delaroche nucleon potentials [27]	3- $\alpha$ OMP-I: $\alpha$ potential of Ref. [37] (Table 1)
	2-McFS: McFadden-Satchler [36] potential	4- $\alpha$ OMP-II: $\alpha$ potential of Ref. [37] (Table 2)
NLD	1-CTM: Constant temperature [29] + Fermi gas model [30]	5- $\alpha$ OMP-III: $\alpha$ potential of Ref. [37] dispersive model
	2-BFM: Back-shifted Fermi gas model [30]	6-Avrigeanu $\alpha$ OMP-II: Avrigeanu <i>et al.</i> potential [38]
	3-GSM: Generalized superfluid model [41]	7-Nolte $\alpha$ OMP: $\alpha$ potential of Nolte <i>et al.</i> [39]
$\gamma$ SF	1-KU: Generalized Lorentzian of Kopecky and Uhl [31]	8-Avrigeanu $\alpha$ OMP: $\alpha$ potential of Avrigeanu <i>et al.</i> [40]
	2-BA: Generalized Lorentzian of Brink and Axel [45,46]	4-MHF: Microscopic level densities on the basis of Hartree-Fock calculations [42]
		5-HCM: Hilaire and Goriely microscopic combinatorial Model [43]
		6-HFB: Microscopic level densities based on temperature-dependent Hartree-Fock-Bogolyubov [44]
		3-HFBQ: Hartree-Fock-BCS-quasiparticle random-phase approximation [47]
		4-HFBT: Hartree-Fock-Bogolyubov-quasiparticle random-phase approximation [47]
		5-HMG: Hybrid model of Goriely [48]
		6-GTHFB: Goriely $T$ -dependent HFB [48]
		7-RMF: $T$ -dependent RMF [48]
		8-GHFB: Gogny D1M HFB+QRPA [48]

borders. For this reaction, by changing OMP for nucleons and  $\alpha$  particles, the cross sections did not change considerably. In the case of  $\gamma$ SF, the cross sections changed by less than 5%. The most effective models were NLDs that caused the major variation in the cross sections. NLDs are determined by the target and residual nuclei properties such as spin, parity, etc. As can be seen, the JLM-Avrigeanu  $\alpha$ OMP-GSM-RMF indicates the upper border up to around 30 MeV and after that JLM-Avrigeanu  $\alpha$ OMP-HFB-GHFB corresponds to the higher cross-section values. From threshold to 32 MeV nuclear calculations show a good agreement with the data by Miyano

*et al.* [8]. There is a significant discrepancy between the measured and calculated cross sections around the peak. From 32 to 50 there is a good consistency between JLM- Avrigeanu  $\alpha$ OMP-GSM-RMF and experimental data. All theoretical calculations predict the measured data well from 50 to 135 MeV.

The radionuclide  $^{206}\text{Po}$  ( $T_{1/2} = 8.8$  d;  $\varepsilon$ : 94.55%; and  $\alpha$ : 5.45%) has a relatively long half-life. The activities were measured after few days of cooling time via 522.47- and 807.38-keV  $\gamma$  rays. There were adequate experimental data due to the long half-life of this radionuclide so that results

TABLE V. Measured cross sections of the  $^{209}\text{Bi}(p, xn)^{207,206,205,204,203}\text{Po}$  and  $^{209}\text{Bi}(p, pxn)^{207,206,205,204,203,202}\text{Bi}$  reactions.  $i$ ,  $c$ ,  $m$ , and  $g$  stand for independent, cumulative cross sections, isomeric, and ground state, respectively.

Product	Type	$\sigma \pm \Delta\sigma$ (mb)				
		$E_p = 62 \pm 2.5$ MeV	$E_p = 72 \pm 2.0$ MeV	$E_p = 82 \pm 1.5$ MeV	$E_p = 91.8 \pm 1.0$ MeV	$E_p = 100.5 \pm 0.5$ MeV
$^{207}\text{Po}$	$i(m+g)$	$127.7 \pm 13.5$	$66.6 \pm 7.2$	$51.5 \pm 5.8$	$47.3 \pm 5.7$	$39.2 \pm 4.7$
$^{206}\text{Po}$	$i$		$127 \pm 13.3$	$87.3 \pm 9.2$	$71.7 \pm 7.5$	$61.4 \pm 6.4$
$^{205}\text{Po}$	$i(m_1 + m_2 + g)$	$363.0 \pm 46.2$	$242.6 \pm 31.8$	$104.4 \pm 13.8$	$80.6 \pm 11.3$	$60.3 \pm 8.1$
$^{204}\text{Po}$	$i$		$341.5 \pm 36.2$	$160 \pm 17.0$	$89.5 \pm 9.5$	$66.7 \pm 7.1$
$^{203}\text{Po}$	$i(m+g)$			$221.7 \pm 29.3$	$157.8 \pm 20.8$	$91.3 \pm 11.9$
$^{207}\text{Bi}$	$i$	$193.1 \pm 20.9$	$163.0 \pm 18.3$	$152.0 \pm 17.9$	$149.0 \pm 18.9$	$125.2 \pm 15.9$
$^{206}\text{Bi}$	$i(m+g)$		$114.2 \pm 12.5$	$109.7 \pm 12.1$	$111.4 \pm 11.8$	$103.5 \pm 10.9$
$^{205}\text{Bi}$	$i$	$92.4 \pm 11.8$	$144.5 \pm 19.0$	$138.6 \pm 18.4$	$143.1 \pm 20.1$	$144.1 \pm 19.5$
$^{204}\text{Bi}$	$i(m_1 + m_2 + g)$		$42.8 \pm 6.2$	$85.0 \pm 12.3$	$100.0 \pm 14.5$	$100.2 \pm 14.5$
$^{203}\text{Bi}$	$i(m+g)$			$71.2 \pm 11.2$	$83.0 \pm 13.0$	$92.3 \pm 14.7$
$^{202}\text{Bi}$	$c$				$237.8 \pm 24.8$	$274.5 \pm 29.0$

TABLE VI. Measured cross sections of the  $^{nat}\text{Pb}(p, xn)$   
 $^{206,205,204,203,202,201}\text{Bi}$  reactions.

Product	Type	$\sigma \pm \Delta\sigma$ (mb)	
		$E_p = 76 \pm 2.0$ MeV	$E_p = 100 \pm 1.0$ MeV
$^{206}\text{Bi}$	$i(m+g)$	$45.9 \pm 4.7$	$28.9 \pm 2.9$
$^{205}\text{Bi}$	$i$	$87.0 \pm 7.0$	$52.3 \pm 5.4$
$^{204}\text{Bi}$	$i(m_1 + m_2 + g)$	$110.6 \pm 15.5$	$59.7 \pm 8.4$
$^{203}\text{Bi}$	$i(m+g)$	$235.2 \pm 30.8$	$77.8 \pm 10.3$
$^{202}\text{Bi}$	$i$	$281.2 \pm 35.8$	$111.1 \pm 11.7$
$^{201}\text{Bi}$	$i(g)^a$	$166.3 \pm 24.8$	$77.2 \pm 11.4$

<sup>a</sup>The isomeric state decays mostly via an electron capture (91.1%) to  $^{201}\text{Tl}$ .

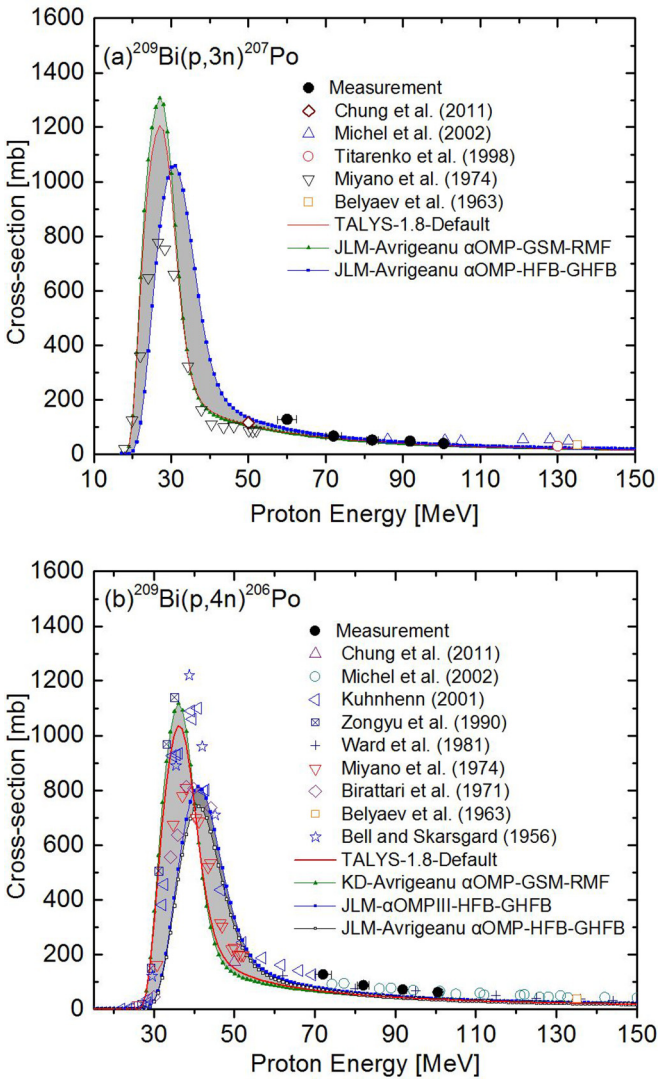


FIG. 3. Independent cross sections for the (a)  $^{209}\text{Bi}(p, 3n)^{207}\text{Po}$ , and (b)  $^{209}\text{Bi}(p, 4n)^{206}\text{Po}$  reactions compared with the earlier experimental data together with theoretical calculations using different model combinations. The experimental data are taken from Refs. [1–10].

from theoretical calculations could be interpreted in details. Figure 3(b) indicates the measured cross sections in this work compared with the theoretical calculations and also the data reported by Chung *et al.* [5], Michel *et al.* [2], Kuhnhen [7], Titarenko *et al.* [1], Zongyu *et al.* [6], Ward *et al.* [9], Miyano *et al.* [8], Birattari *et al.* [10], Belyaev *et al.* [4], and Bell and Skarsgard [3]. Measured cross sections in this work are consistent with the cross sections measured by Kuhnhen [7], Michel *et al.* [2], and Ward *et al.* [9] in the investigated energy range. Furthermore, it can be seen that the theoretical calculations vary significantly by changing the input parameters. In Fig. 3(b), the combinations which produce the high and low values as well as the default calculations are shown. Similarly, no single combination was correspondent to the lower and upper border of the calculated cross sections. The experimental data are in the range of the theoretical calculations from threshold to almost 55 MeV. The nuclear model calculations underestimate the measured data slightly from 55 to 150 MeV. In the calculations, OMP for proton, neutron, and  $\alpha$  particles were changed and no significant effects were observed. It is not surprising, because of low cross-cross sections of ( $p, \alpha$ ) channel. The cross sections vary by less than a few percent when different  $\gamma$ SFs were applied. The notable changes were observed when the NLD changed, in particular, from phenomenological to microscopic ones. As it is shown in Fig. 3(b), the combination JLM-Avrigeanu  $\alpha$ OMP-HFB-GHFB, which includes microscopic NLDs, produces the minimum cross sections with respect to the peak. On the other hand, the KD-Avrigeanu  $\alpha$ OMP-GSM-RMF, which includes phenomenological NLDs, produces the maximum cross sections. These results emphasize the importance of the nuclear properties such as spin, parity, and other parameters of the nuclei involved in the reaction.

### B. $^{209}\text{Bi}(p, 5n)^{205}\text{Po}$ and $^{209}\text{Bi}(p, 6n)^{204}\text{Po}$ reactions

Activities of short-lived radionuclide  $^{205}\text{Po}$  ( $T_{1/2} = 1.74$  h;  $\epsilon: 99.96\%$ ; and  $\alpha: 0.04\%$ ) were measured after almost half an hour of cooling time via 836.8, 849.8, and 872.4 keV  $\gamma$  rays. One can notice that the measured activity included the contribution of the decay of the simultaneously produced short-lived isomeric states ( $T_{1/2} = 57.4$  ms; IT: 100%, and  $T_{1/2} = 0.64$  ms; IT: 100%). Shown in Fig. 4(a) are the data in this work together with the other reported data by Chung *et al.* [5], Titarenko *et al.* [1], Belyaev *et al.* [4], and Bell and Skarsgard [3], and theoretical calculations by TALYS. There were no experimental data in the investigated energy range so that these data were the first ones. According to Fig. 4(a), measured data in this work continue the shape of the results reported by Bell and Skarsgard [3] well. In addition, our data seem to have a similar trend as that reported by Titarenko *et al.* [1] and Belyaev *et al.* [4]. Similar to other reactions, all the possible combinations were applied to the TALYS code to observe the variation of the cross sections. In Fig. 4(a), the models corresponding to the high and low cross section values are indicated. Results from the calculations cover the data of Ref. [3] from 40 to 50 MeV and after that there is some deviation. TALYS1.8-Default shows the maximum cross section as 799 mb at 45 MeV while that

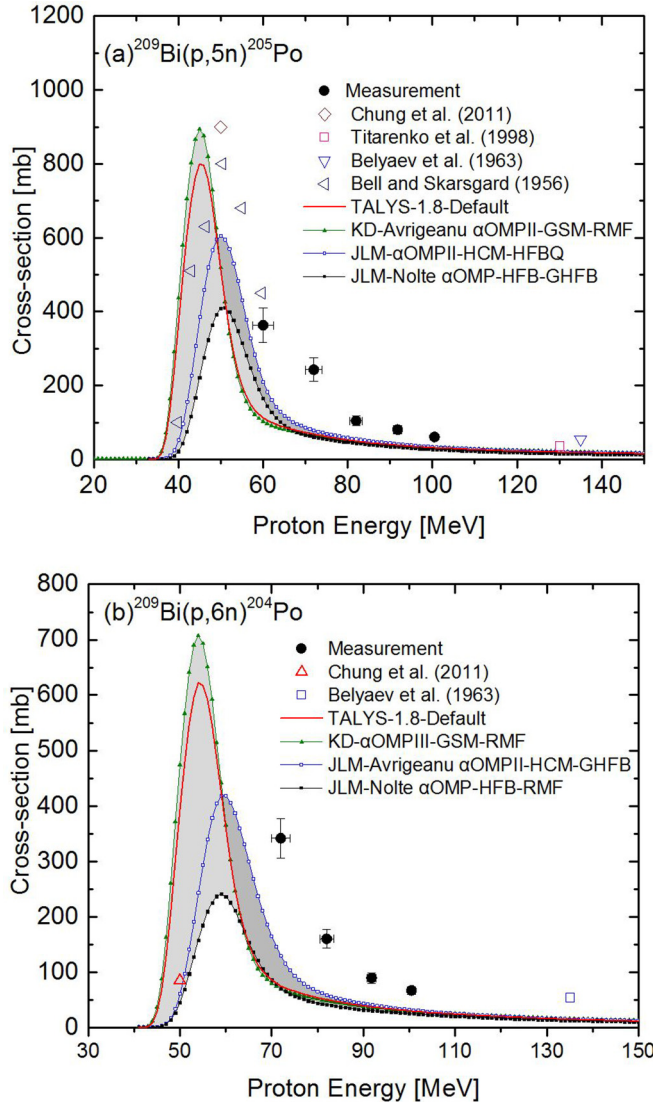


FIG. 4. Independent cross sections for the (a)  $^{209}\text{Bi}(p, 5n)^{205}\text{Po}$ , and (b)  $^{209}\text{Bi}(p, 6n)^{204}\text{Po}$  reactions compared with the earlier experimental data together with theoretical calculation model combinations. The experimental data are taken from Refs. [1,3–5].

of Bell and Skarsgard [3] is 800 mb at 50.4 MeV. For the  $^{209}\text{Bi}(p, 5n)^{205}\text{Po}$  reaction, OMPs were not effective, however, the  $\gamma$ SFs made a few-percent contribution to the cross-section variation. By changing the different models, it was observed that phenomenological NLD models presented considerably different cross sections from the microscopic ones. For this reaction, JLM-Nolte  $\alpha$ OMP-HFB-GHFB models predict the lowest cross sections regarding to the peak value, whereas, KD-Avrigeanu  $\alpha$ OMPII-GSM-RMF estimates the highest cross sections. The TALYS default is near the peak due to use of the CTM+FGM as the level density model.

The cross sections of short-lived radionuclide  $^{204}\text{Po}$  ( $T_{1/2} = 3.519\text{ h}$ ;  $\epsilon : 99.33\%$ ; and  $\alpha : 0.67\%$ ) were also measured by using 270.07 keV  $\gamma$  ray that was well defined in the spectrum of each bismuth irradiated foil. The measured experimental cross sections are indicated in Fig. 4(b) compared with earlier

experimental data found in the literature and results from theoretical calculations. There were two single points reported by Chung *et al.* [5] and Belyaev *et al.* [4] at 50 and 135 MeV, respectively. Therefore, the cross sections for the reaction  $^{209}\text{Bi}(p, 3n)^{204}\text{Po}$  were measured for the first time in the energy range of 70 to 100 MeV. As can be seen from the figure, between 50 and 70 MeV no experimental data exist so it is necessary to conduct experiments to fill this gap. On the other hand, the theoretical calculations could play a leading role for this energy range. Results from the TALYS code using different models show very large variations in the cross sections. In the calculations, by fixing the other nuclear ingredients and changing one input, it was observed that the reason for variation in the cross section was NLD models in addition to around 5% resulting from different  $\gamma$ SFs. We can see that the JLM-Avrigeanu  $\alpha$ OMPII-HCM-GHFB predicts the data by Chung *et al.* [5] well and it produces the upper border after 60 MeV. Similar to the previous reactions, there is a big change by switching between NLD especially from the phenomenological to microscopic. The TALYS default shows an incorrect threshold for this reaction. In the high energy range, the experimental data are underestimated by all model combinations.

### C. $^{209}\text{Bi}(p, 7n)^{203}\text{Po}$ and $^{209}\text{Bi}(p, p2n)^{207}\text{Bi}$ reactions

$^{203}\text{Po}$  has a ground state ( $T_{1/2} = 36.7\text{ m}$ ;  $\epsilon : 99.89\%$ ; and  $\alpha : 0.11\%$ ) and an isomeric state ( $T_{1/2} = 45\text{ s}$ ; IT: 100%) which decays to the ground state via an IT process. Therefore, the measured activity is contributed by both the ground and isomeric states. The activity for the short-lived radionuclide  $^{203}\text{Po}$  was measured by using the 1090.9-keV  $\gamma$  ray. The excitation functions are shown in Fig. 5(a) together with the data obtained by Titarenko *et al.* [1] at 130 MeV and Belyaev *et al.* [4] at 135 MeV. It can be inferred that our data and measured cross sections by Titarenko *et al.* [1] and Belyaev *et al.* [4] follow almost a similar trend. In this reaction, seven neutrons are emitted which makes it a complex reaction so it is expected to observe a discrepancy between theoretical and experimental data. The results from the TALYS with changes in the cross sections are also denoted in Fig. 5(a). The maximum cross sections are obtained by using KD- $\alpha$ OMPIII-GSM-HFBQ and the minimum cross sections are from the KD-Avrigeanu  $\alpha$ OMPII-MHF-HFBQ. It was noted that using various OMPs were not effective and applying  $\gamma$ SFs were effective by a few percent. The most vital input model was NLD. However, the theoretical predictions are not reasonable in the investigated energy range. The importance of carrying out new experiments around the peak area is quite obvious to benchmark nuclear input ingredients.

$^{207}\text{Bi}$  ( $T_{1/2} = 31.55\text{ yr}$ ,  $\epsilon : 100\%$ ) was measured by its 569.698-keV  $\gamma$  ray. There was only one independent cross section data set including a single point at 135 MeV, which was reported by Belyaev *et al.* [4]. It can be deduced that our measured cross sections and that of Belyaev *et al.* [4] are on the same trend. For this reaction, theoretical calculations with all possible model combinations were done by TALYS and the results are shown in Fig. 5(b). The upper values of the cross sections were estimated by JLM-Avrigeanu  $\alpha$ OMP-HFB-GHFB

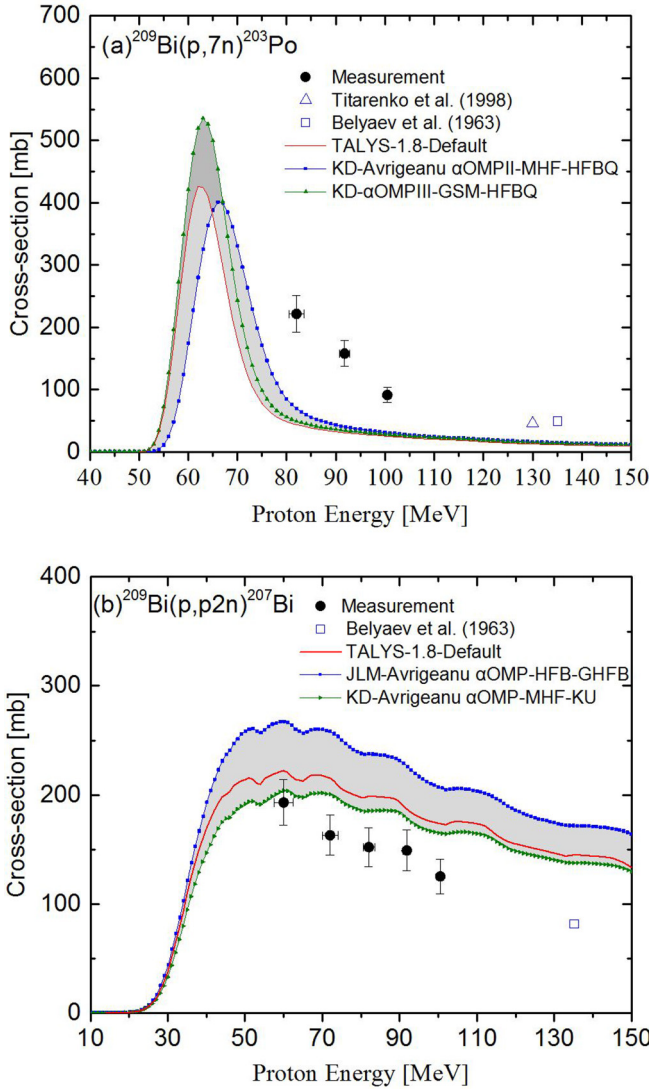


FIG. 5. Independent cross sections for the (a)  $^{209}\text{Bi}(p, 7n)^{203}\text{Po}$ , and (b)  $^{209}\text{Bi}(p, p2n)^{207}\text{Bi}$  reactions compared with the earlier experimental data together with theoretical calculations using model combinations. The experimental data are taken from Refs. [1,4].

and that of lower border by KD-Avrigeanu  $\alpha$ OMP-MHF-KU. The most important input parameter was NLD, particularly switching between microscopic and phenomenological models. Even so, different  $\gamma$ SFs contributed to the change of cross section almost by a few percent. Other input parameters made almost no change in the cross sections. It can be seen that results from KD-Avrigeanu  $\alpha$ OMP-MHF-KU are closer to the experimental data over the whole energy range. This reaction needs more experimental data from 30 to 60 MeV.

#### D. $^{209}\text{Bi}(p, p3n)^{206}\text{Bi}$ and $^{nat}\text{Pb}(p, xn)^{206}\text{Bi}$ reactions

The independent cross sections of the reaction  $^{209}\text{Bi}(p, p3n)^{206}\text{Bi}$  were measured.  $^{206}\text{Bi}$  has two states: a ground state ( $T_{1/2} = 6.243\text{ d}; \epsilon : 100\%$ ) and a very short-lived isomeric state ( $T_{1/2} = 0.89\text{ ms}$ ), which decays completely to the ground state by an IT process. The production of  $^{206}\text{Bi}$  is also

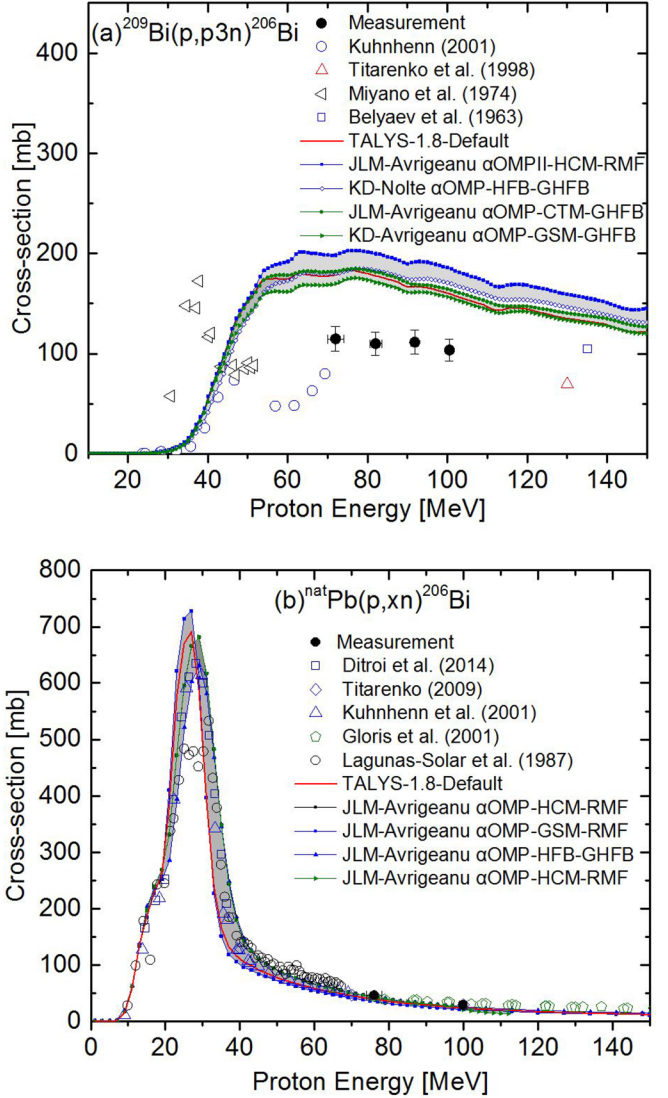


FIG. 6. Independent cross sections for the (a)  $^{209}\text{Bi}(p, p3n)^{206}\text{Bi}$ , and (b)  $^{nat}\text{Pb}(p, xn)^{206}\text{Bi}$  reactions compared with the earlier experimental data together with theoretical calculations using model combinations. The experimental data are taken from Refs. [1,4,7,8,11,13,14,16].

contributed by decay of  $^{206}\text{Po}$  which is produced in the investigated energy region. The activity of  $^{206}\text{Bi}$  was measured by its 803.10, 881.01, and 516.18 keV  $\gamma$  rays. The results are illustrated in Fig. 6(a) together with other independent cross sections reported by Kuhnhen [7], Titarenko *et al.* [1], Miyano *et al.* [8], and Belyaev *et al.* [4]. Our data slightly overestimate the data reported in [7]. Moreover, over the energy range of 70 to 100 MeV our measured cross sections are new and it can also be assumed that measured data by Titarenko *et al.* [1] at 130 MeV follow a similar trend as the results presented in this work. Data reported by Miyano *et al.* [8] are accumulated around 30 to 40 MeV. Similar to preceding reactions, an extensive calculation was conducted by TALYS code to figure out the ability of nuclear model calculations. As shown in the figure, there are two band regions which resulted

from different models in TALYS calculation. The different results are obtained when the NLD model changes. No big effects from various OMPs and  $\gamma$ SFs were observed. From the threshold, theoretical calculations are consistent with the data reported by Kuhnhen [7], while, by increasing the energy, the discrepancy between calculations and measurements becomes noticeable.

In order to see the effects of nuclear properties on the reactions including heavy nuclei, the production cross sections of the reaction  ${}^{nat}\text{Pb}(p, xn){}^{206}\text{Bi}$  were measured and the results were compared to the earlier reported data and the theoretical results [Fig. 6(b)]. A very good agreement is observed between our data and data provided by Gloris *et al.* [11] and also the theoretical calculations. In the case of prediction of nuclear models, it can be seen that almost all recent experimental data are in the range of theoretical calculations, except for the data reported by Lagunas-Solar *et al.* [13] at around 30 MeV. Around the peak area, theoretical calculations using JLM-Avrigeanu  $\alpha$ OMP-HFB-GHFB predicts the measured data well.

#### E. ${}^{209}\text{Bi}(p, p4n){}^{205}\text{Bi}$ and ${}^{nat}\text{Pb}(p, xn){}^{205}\text{Bi}$ reactions

The long-lived radionuclide  ${}^{205}\text{Bi}$  ( $T_{1/2} = 15.31$  d;  $\varepsilon : 100\%$ ) was produced via  ${}^{209}\text{Bi}(p, p4n){}^{205}\text{Bi}$  reaction and through the decay of short-lived radionuclide  ${}^{205}\text{Po}$  ( $T_{1/2} = 1.74$  h). Therefore, the measured activities are cumulative. The production cross sections for the reaction  ${}^{209}\text{Bi}(p, p4n){}^{205}\text{Bi}$  were measured by the 703.45-keV  $\gamma$  ray that was visible in the spectrum of each  ${}^{209}\text{Bi}$  irradiated foil after several days. The results of this work are compared with existing measurements and TALYS calculations. By calculating the cross sections using different nuclear models, three bands were produced for which the corresponding combination is indicated in Fig. 7(a). The lower band was created by different OMPs of proton, neutron, and  $\alpha$  particles, while the two upper bands were produced mostly when different NLDs were used. It seems that for the low energy range the lower band predicts the data well, whereas for higher energies the upper bands are consistent with the data in this work and that of Belyaev *et al.* [4]. From 70 to 140 MeV, the theoretical calculations connect two experimental data which means we can rely on the nuclear model calculation as no experimental data exist from 100 to 140 MeV. Nevertheless, further measurements for the reaction  ${}^{209}\text{Bi}(p, p4n){}^{205}\text{Bi}$  at proton energies higher than 100 MeV are required.

Excitation functions of the  ${}^{nat}\text{Pb}(p, xn){}^{205}\text{Bi}$  reactions at energies of 100 and 76 MeV were also determined. The cross sections were measured by Ditrói *et al.* [14], Titarenko *et al.* [16], Kuhnhen [7], and Gloris *et al.* [11,12]. As can be seen from Fig. 7(b) our data correspond well with the cross sections in Refs. [7,11,12]. Theoretical calculations are also shown in the figure. As it can be seen, three bands were created by different models so that the first two bands from the bottom are created when different  $\alpha$ OMPs with the level density models HFB and HCM were used. On the other hand, the upper band was produced when phenomenological NLDs, MHFs, and different  $\alpha$ OMPs were used. For this reaction, the  $(p, \alpha)$  channel seems to be open according to the sensitivity of the

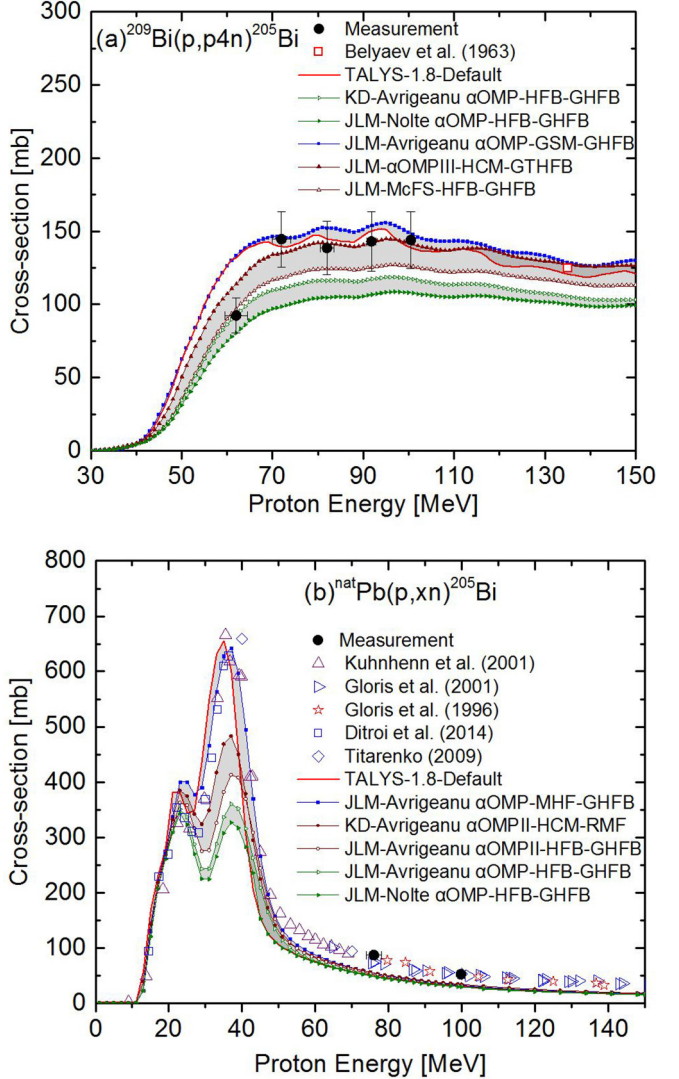


FIG. 7. Independent cross sections for the (a)  ${}^{209}\text{Bi}(p, p4n){}^{205}\text{Bi}$ , and (b)  ${}^{nat}\text{Pb}(p, xn){}^{205}\text{Bi}$  reactions compared with the earlier experimental data together with theoretical calculations model combinations. The experimental data are taken from Refs. [4,7,11,14,16].

cross sections to the  $\alpha$ OMPs.  $\gamma$ -ray strength functions made a small change in the cross sections. From the figure, we can see that the experimental data are predicted well by the upper band over the whole energy range.

#### F. ${}^{209}\text{Bi}(p, p5n){}^{204}\text{Bi}$ and ${}^{nat}\text{Pb}(p, xn){}^{204}\text{Bi}$ reactions

The radionuclide  ${}^{204}\text{Bi}$  ( $T_{1/2} = 11.22$  h;  $\varepsilon : 100\%$ ) was produced through the  ${}^{209}\text{Bi}(p, p5n){}^{204}\text{Bi}$  reaction. The measured activity included the contribution of the decay of the simultaneously produced short-lived isomeric states ( $T_{1/2} = 13$  and 1 ms, 100% IT) and also the decay of its parent  ${}^{204}\text{Po}$  ( $T_{1/2} = 3.519$  h). The  ${}^{204}\text{Bi}$  radionuclide was identified by 374.76-keV  $\gamma$  ray. The measured cross sections for the production of  ${}^{204}\text{Bi}$  are denoted in Fig. 8(a). Similar to the previous reaction, the independent cross section was only measured by Belyaev *et al.* [4] at 140 MeV. From the figure, the lowest border of the cross-section values are predicted

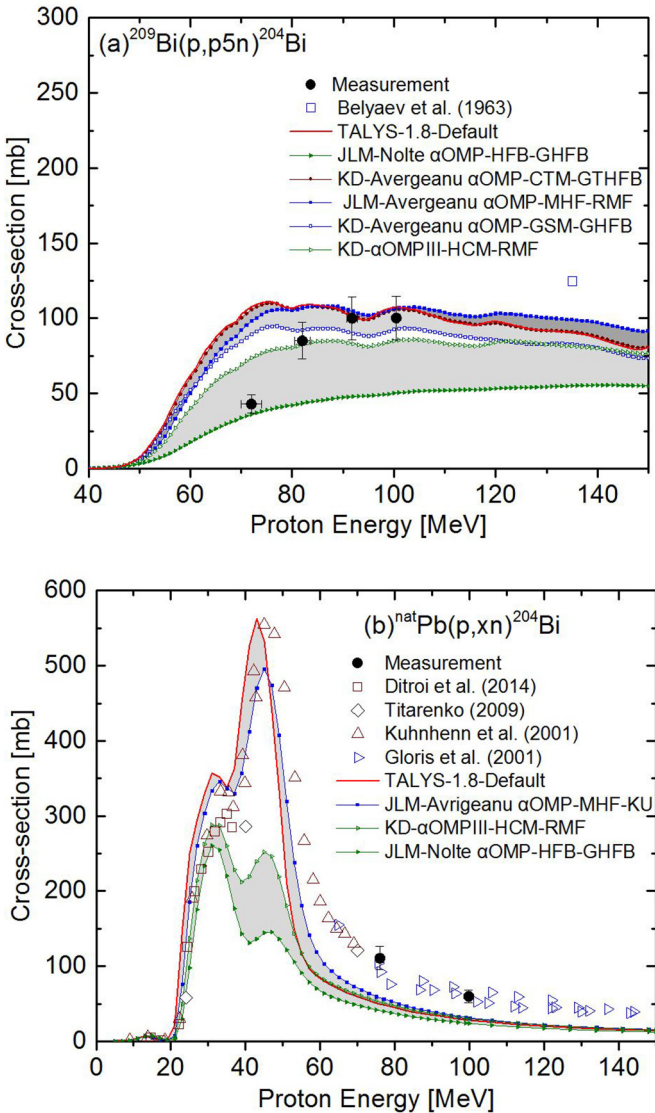


FIG. 8. Independent cross sections for the (a)  $^{209}\text{Bi}(p, p5n)^{204}\text{Bi}$ , and (b)  $^{\text{nat}}\text{Pb}(p, xn)^{204}\text{Bi}$  reactions compared with the earlier experimental data together with theoretical calculations using different model combinations. The experimental data are taken from Refs. [4,7,11,14,16].

by JLM-Nolte  $\alpha$ OMP-HFB-GHFB and the highest ones by TALYS1.8-Default + JLM-Avergeanu  $\alpha$ OMP-MHF-RMF. The OMPs were not very effective for this reaction and  $\gamma$ SFs had a small contribution to the values. It can result that the most important ingredient could be spin, parity, etc. of the compound nucleus which are determined from tables or NLD models. Due to a large variation in the cross sections it was not easy to conclude which model could predict the experimental data reasonably. However, around 90–100 MeV our data are predicted well by the TALYS default calculations. At higher energies, nuclear models underestimate the data by Ref. [4]. It is also recommended to conduct more experiments below 80 MeV and above 100 MeV.

Excitation functions for the  $^{\text{nat}}\text{Pb}(p, xn)^{204}\text{Bi}$  reactions were also obtained and the results were compared with the

previously reported values by Detroi *et al.* [14], Titarenko *et al.* [16], Kuhnhen [7], and Gloris *et al.* [11] together with the theoretical model calculations [Fig. 8(b)]. Our values show a satisfactory consistency with the cross sections published by Gloris *et al.* [11]. In addition, calculated cross sections predict the shape of the excitation functions well. However, there is a big gap in the cross sections using different models. From the figure, the lower band results from using KD- $\alpha$ OMP III-HCM-RMF and JLM-Nolte  $\alpha$ OMP-HFB-GHFB. By considering different combinations, it was observed that the most effective models were NLDs and the least important were OMPs, while,  $\gamma$ SFs were in the middle. By using the combinations including HCM and HFB, it was realized that the smaller values are produced than the combinations including the other NLD models. This might be because of the descriptions of the nuclear properties provided by HCM and HFB in the TALYS database which need to be refined. Overall, all nuclear models predict the threshold well, and the upper band estimates the measured data well both in shape and order of the magnitude up to around 60 MeV, underestimating the data after 60 MeV.

#### G. $^{209}\text{Bi}(p, p6n)^{203}\text{Bi}$ and $^{\text{nat}}\text{Pb}(p, xn)^{203}\text{Bi}$ reactions

Activities of short-lived  $^{203}\text{Bi}$  ( $T_{1/2} = 11.76$  h;  $\varepsilon : 100\%$ ) were measured after few hours of cooling time via a 820.2-keV  $\gamma$  ray. The measured activities contributed by the decay of the simultaneously produced short-lived isomeric state ( $T_{1/2} = 305$  ms; IT: 100%) and also the decay of  $^{203}\text{Po}$  ( $T_{1/2} = 36.7$  m). The activities of the parent were measured in three Bi foils. However, the  $^{203}\text{Po}$  half-life was short; we could measure independent activities of  $^{203}\text{Bi}$  radionuclide. Figure 9(a) indicates the cross sections of the reaction  $^{209}\text{Bi}(p, p6n)^{203}\text{Bi}$  measured in this work together with data of Ref. [4] in comparison with the theoretical results. The combinations including HCM or HFB nuclear densities estimated low cross sections which means these nuclear tables need to be modified for the produced compound nucleus or  $^{203}\text{Bi}$ . On the other hand, it can be seen that the upper band is created when a phenomenological NLD is used; the cross sections are comparable to the measured data. Even so, there is an underestimation of the experimental data at 140 MeV. Other nuclear parameters were less effective to this reaction. It is stressed that more experimental data are required.

The cross sections of the  $^{\text{nat}}\text{Pb}(p, xn)^{203}\text{Bi}$  reaction were measured. For this case, adequate experimental data could be found in the literature [7,11,14,16]. The consistency of data measured in this work with that of Gloris *et al.* [11] is significant at 100 MeV, while our data overestimate those data around 75 MeV [Fig. 9(b)]. Theoretical calculations show different results by using different models. In this case, almost all input parameters were less effective than the NLD models, although all models predict the experimental data at the threshold well. The upper band is in a good agreement with the data both in shape and order of magnitude up to 60 MeV. All the models decrease more rapidly than the experimental data from 60 MeV up to 150 MeV. Using HFB or HCM as the level densities produced the lower band, while other NLD models correspond to the upper band. As a result, the HFB and HCM models needs more modifications.

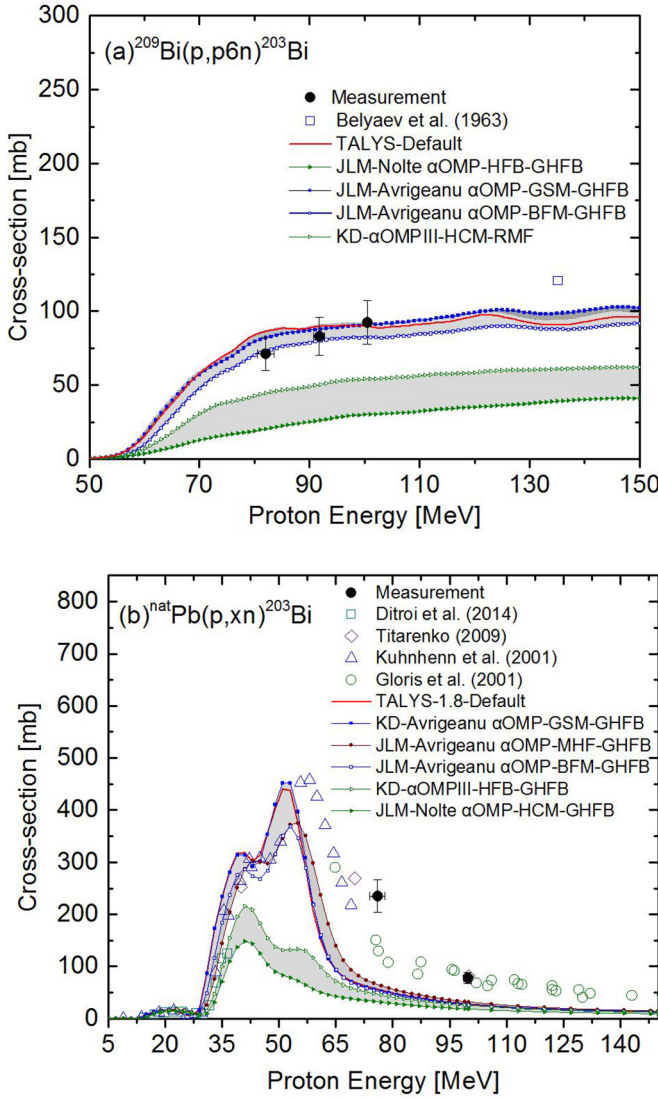


FIG. 9. Independent cross sections for the (a)  $^{209}\text{Bi}(p, p6n)^{203}\text{Bi}$ , and (b)  $^{nat}\text{Pb}(p, xn)^{203}\text{Bi}$  reactions compared with the earlier experimental data together with theoretical calculations using different model combinations. The experimental data are taken from Refs. [4,7,11,14].

#### H. $^{209}\text{Bi}(p, p7n)^{202}\text{Bi}$ , $^{nat}\text{Pb}(p, xn)^{202}\text{Bi}$ and $^{nat}\text{Pb}(p, xn)^{201}\text{Bi}$ reactions

The production cross sections of the radionuclide  $^{202}\text{Bi}$  ( $T_{1/2} = 1.71\text{ h}$ ;  $\epsilon : 100\%$ ) through the  $^{209}\text{Bi}(p, p7n)^{202}\text{Bi}$  reaction were measured after almost half an hour of cooling time via 657.49- and 960.67-keV  $\gamma$  rays. In this case, because there were no  $\gamma$  rays for  $^{202}\text{Po}$  (44.6 m) parent nuclide, the activity of the parent could not be measured. Therefore, obtained cross sections were cumulative. The results of this work together with the earlier data and theoretical calculations are illustrated in Fig. 10(a). In order to consider the consistency of theoretical calculations with the experimental data, the cross sections of  $^{209}\text{Bi}(p, p7n)^{202}\text{Bi}$  and  $^{209}\text{Bi}(p, 8n)^{202}\text{Po}$  reactions were added because the production cross sections of the reaction  $^{209}\text{Bi}(p, 8n)^{202}\text{Po}$  were significant over the investigated energy range.

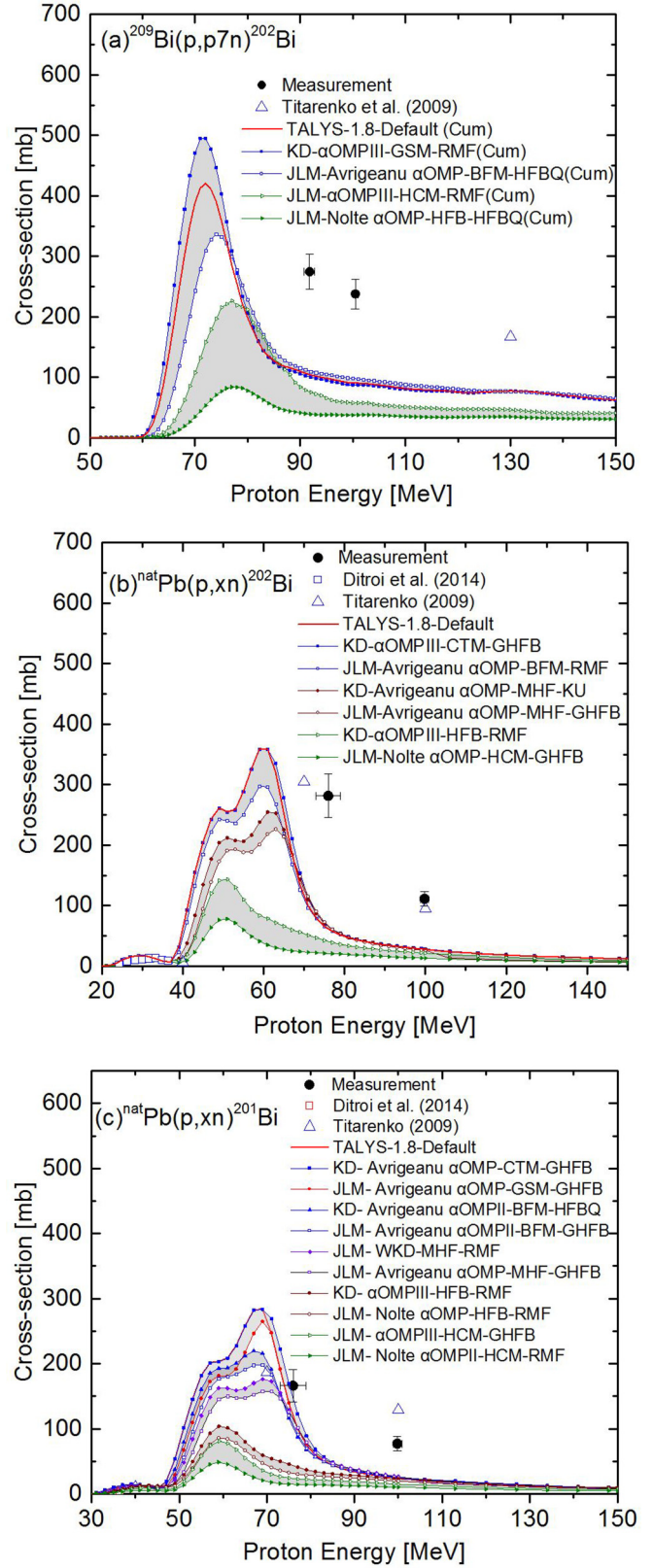


FIG. 10. Cumulative cross sections for the (a)  $^{209}\text{Bi}(p, p6n)^{202}\text{Bi}$ , (b)  $^{nat}\text{Pb}(p, xn)^{202}\text{Bi}$ , and (c)  $^{nat}\text{Pb}(p, xn)^{201}\text{Bi}$  reactions compared with the earlier experimental data together with theoretical calculations using different model combinations. The experimental data are taken from Ref. [14,16].

Titarenko *et al.* [1] published cross section for this reaction at 135 MeV. Obviously, our data and that of Ref. [1] could be on an almost similar trend. From Fig. 10(a), there are two bands which correspond to different input parameters. The effects of all input models were considered and it was found out that OMPs and  $\gamma$ SFs were not significant. The major variation in the cross sections resulted from using different NLDs, the highest values predicted by GSM and the lowest ones predicted by HFB. Clearly, in the investigated energy range all theoretical calculations fail to estimate reasonable values. However, more experiments on this reaction around 60–90 MeV are vital for a better understanding of the models' predictions.

The production cross sections for the  $^{nat}\text{Pb}(p, xn)^{202}\text{Bi}$  reaction were also measured. For this reaction, there were two experimental datasets reported by Ditzoi *et al.* [14] and Titarenko *et al.* [16]. Cross sections measured in this study and those of Refs. [14] and [16] as well as results from theoretical calculations are shown in Fig. 10(b). As can be seen from the figure, our results agree with those of Titarenko *et al.* [16]. Nuclear model calculations for this reaction showed three bands in the cross sections. The lowest band was produced by JLM-Nolte  $\alpha$ OMP-HCM-GHFB and KD- $\alpha$ OMPIII-HFB-RMF in which the major alteration stems from the NLD. The middle band was produced by JLM-Avrigeanu  $\alpha$ OMP-MHF-GHFB and KD-Avrigeanu  $\alpha$ OMP-MHF-KU which shows the effect of different OMPs. The upper band was created by JLM-Avrigeanu  $\alpha$ OMP-BFM-RMF and KD- $\alpha$ OMPIII-CTM-GHFB in which NLD corresponded to the most variation. It is clear that the lowest band including HCM and MHF is not able to predict the data for the production of  $^{202}\text{Bi}$ . However, the theoretical calculations could estimate the measured data around threshold. They could not predict the experimental data in the investigated energy range. Since no data are available from 40 to 70, it is highly recommended to conduct experiments in this range, helping to benchmark nuclear model calculations.

The  $^{201}\text{Bi}$  has two states with almost similar half-lives, including  $^{201g}\text{Bi}$  ( $T_{1/2} = 103\text{ m}$ ;  $\epsilon : 100\%$ ) and  $^{201m}\text{Bi}$  ( $T_{1/2} = 57.5\text{ m}$ ;  $\epsilon : > 91.1\%$ ; IT:  $\leq 8.6\%$ ;  $\alpha \approx 0.3\%$ ). It should be noticed that a small part of the isomeric state decays to the ground state via an IT process. Therefore, the measured cross sections can be partially contributed by this process. The isomeric state decays mostly via an electron capture process to  $^{201}\text{Tl}$ . The activity of this short-lived radionuclide  $^{201}\text{Bi}$  was measured via 629.1-keV  $\gamma$  ray. The experimental and theoretical cross sections are depicted in Fig. 10(c). Data in this work are overestimated by that of Titarenko *et al.* [16]. The results show five bands of which the correspondent combination is indicated in the figure. Each band is produced by different NLDs and the variation of each band is resulted from different OMPs or  $\gamma$ SFs. From the bottom, the bands were produced by HCM, HFB, MHF, BFM, and GSM + CTM. For this reaction, the most important parameters were NLDs. From the figure, theoretical data predict the threshold well. JLM-

Avrigeanu  $\alpha$ OMPII-BFM-GHFB estimates data by Titarenko *et al.* [16] at 70 MeV, while KD-Avrigeanu  $\alpha$ OMP-CTM-GHFB predicts our data at 80 MeV. Therefore, no specific model could be concluded as the best model. It seems that some experiments are needed for the energy range of 40 to 100 MeV.

#### IV. CONCLUSIONS

In this study, the cross sections for proton-induced reactions on bismuth and lead were measured up to 100 MeV. These data were deduced from the activation analysis method in two rounds of experiments to extend the experimental database toward heavy nuclei. About 40 new cross sections were measured over the energy range of 60–100 MeV and were compared to other published data and theoretical calculations. Our data were in good agreement with the data existing in the literature.

Hereby, the most updated libraries were used for the nuclear ingredients. Semimicroscopic and phenomenological optical model potentials (OMPs), different nuclear level densities (NLDs), and  $\gamma$ -ray strength functions ( $\gamma$ SFs) were tested. The effects of the mentioned models on the cross sections could not be neglected. There is no unique combination which is able to describe the experimental data. However, in most cases the combinations including HCM and HFB as the nuclear level densities produced very low values, while, the other NLDs could produce more reasonable data. For the proton-induced reaction on Bi the effects of OMPs were negligible and those of  $\gamma$ SFs were a few percent. The most of the variation in the cross sections came from different NLDs. In the case of the proton-induced reaction on Pb,  $\alpha$ OMPs became effective by a few percent similar to the  $\gamma$ SFs. However, NLDs still played the leading role. In the case of reactions in which more neutrons are emitted, the theoretical calculations are more deviated from the experimental data. Especially, the threshold energies predicted by theoretical models are different from the measured data for the  $(p, pxn)$  reactions. Overall, our results reveal the pressing need for the study on proton-induced reactions up to 100 MeV or higher energy range to test the nuclear ingredients such OMPs, NLDs, and  $\gamma$ SFs.

#### ACKNOWLEDGMENTS

We are pleased to acknowledge the cooperation of operation team at KOMAC in performing the irradiation and we also thank our colleague O. Bae for his considerable help. This work was supported by the Nuclear Safety Research Program through the Korea Foundation Of Nuclear Safety (KOFONS), granted financial resource from the Nuclear Safety and Security Commission (NSSC), and of Republic of Korea (Grants No. 1303026 and No. 1603005).

- [1] Y. E. Titarenko, O. V. Shvedov, M. M. Igumnov, S. G. Mashnik, E. I. Karpikhin, V. D. Kazaritsky, V. F. Batyaev, A. B. Koldobsky, V. M. Zhivun, A. N. Sosnin, R. E. Prael, M. B. Chadwick, T. A. Gabriel, and M. Blann, Experimental and computer simulation study of the radionuclides produced in thin 209-Bi targets by 130 MeV and 1.5 GeV proton-induced reactions, *Nucl. Instrum. Methods Phys. Res. A* **414**, 73 (1998).
- [2] R. Michel, M. Gloris, J. Protoschill, U. Herpers, J. Kuhnhenn, F. Sudbrock, P. Malmborg, and P. Kubik, Cross sections for the production of radionuclides by proton-induced reactions on W, Ta, Pb and Bi from thresholds up to 2.6 GeV, *J. Nucl. Sci. Technol.* **34**, 242 (2002).
- [3] R. E. Bell, and H. M. Skarsgard, Cross sections of (p, xn) reactions in the isotopes of lead and bismuth, *Can. J. Phys.* **34**, 745 (1956).
- [4] B. I. Belyaev, A. V. Kalyamin, and A. N. Murin, Excitation functions of nuclear reactions, occurring at bombardment Bi-209 by fast protons, *Bull. Russ. Acad. Sci. Phys.* **27**, 907 (1963).
- [5] Y. H. Chung, C. S. Lee, K. Y. Nahm, K. S. Joo, J. S. Chai, and K. S. Chun, Cross sections of bismuth and polonium isotopes in the reaction of <sup>209</sup>Bi with protons, *J. Kor. Phys. Soc.* **59**, 1007 (2011).
- [6] B. Zongyu, C. J. Inhua, M. Jiangchen, and H. Shengnian, The measurement of the ratio gamma-F/gamma-n and the fission barrier height for p+Bi-209, *Chin. J. Nucl. Phys.* **12**, 55 (1990).
- [7] J. Kuhnhenn, Thin target cross sections for proton-induced production of radionuclides from lead and bismuth over the proton energy range from 9 to 71 MeV, Ph.D thesis, University of Koeln, 2001.
- [8] K. Miyano, M. Sekikawa, T. Kaneko, and M. Nomoto, Reactions on <sup>209</sup>Bi induced by intermediate energy protons and the effect of direct reactions, *Nucl. Phys. A* **230**, 98 (1974).
- [9] T. E. Ward, P. P. Singh, D. L. Friesel, A. Yavin, A. Doron, J. M. D. Auria, G. Sheffer, and M. Dillig, Radiochemical study of the combined (p,  $\pi^0$ ) and (p,  $\gamma$ ) reactions on bismuth with protons from 62 to 480 MeV, *Phys. Rev. C* **24**, 588 (1981).
- [10] C. Birattari, E. Gadioli, A. M. Grassi Strini, G. Strini, G. Tagliaferri, and L. Zetta, (p, xn) Reactions induced in <sup>169</sup>Tm, <sup>181</sup>Ta and <sup>209</sup>Bi with 20 to 45 MeV protons, *Nucl. Phys. A* **166**, 605 (1971).
- [11] M. Gloris, R. Michel, F. Sudbrock, U. Herpers, P. Malmborg, and B. Holmqvist, Proton-induced production of residual radionuclides in lead at intermediate energies, *Nucl. Instrum. Methods Phys. Res. A* **463**, 593 (2001).
- [12] M. Gloris, R. Michel, U. Herpers, F. Sudbrock, and D. Filges, Production of residual nuclei from irradiation of thin Pb-targets with protons up to 1.6 GeV, *Nucl. Instrum. Methods Phys. Res. B* **113**, 429 (1996).
- [13] M. C. Lagunas-Solar, O. F. Carvacho, L. Nagahara, A. Mishra, and N. J. Parks, Cyclotron production of no-carrier-added <sup>206</sup>Bi (6.24 d) and Bi (15.31 d) as tracers for biological studies and for the development of alpha-emitting radiotherapeutic agents, *Appl. Radiat. Isot.* **38**, 129 (1987).
- [14] F. Ditroi, F. Tárkányi, S. Takács, and A. Hermanne, Proton-induced cross sections of nuclear reactions on lead up to 37 MeV, *Appl. Radiat. Isot.* **90**, 208 (2014).
- [15] C. Brun and M. Lefort, Production of polonium isotopes 196 to 202 by (p, xn) nuclear reactions on bismuth, *J. Inorg. Nucl. Chem.* **26**, 1633 (1964).
- [16] Y. E. Titarenko, V. F. Batyaev, E. I. Karpikhin, V. M. Zhivun, A. V. Ignatyuk, V. P. Luney, N. N. Titarenko, Yu. N. Shubin, and V. S. Barashenkov, Experimental and theoretical studies of the yields of residual product nuclei produced in thin Pb and Bi targets irradiated by 40-2600 MeV protons, IAEA, Nuclear Data Section, INDC(CCP)-0447 (2009), [https://inis.iaea.org/search/search.aspx?orig\\_q=RN:43028605](https://inis.iaea.org/search/search.aspx?orig_q=RN:43028605).
- [17] A. J. Koning, S. Hilaire, and S. Goriely, TALYS-1.8: A nuclear reaction program. User manual, NRG, Netherlands, Access December 2015, <http://www.talys.eu/download-talys>.
- [18] M. Bakhtiari, M. Sadeghi, M. K. Bakht, and H. Ghafoori-Fard, Nuclear model calculations of charged particle induced reaction cross section data for the production of the radiohalogen <sup>34m</sup>Cl, *Phys. Rev. C* **87**, 034621 (2013).
- [19] M. Sadeghi, M. Bakhtiari, M. K. Bakht, M. Anjomrouz, and L. Mokhtari, An overview of mercury radionuclides and nuclear model calculations of <sup>195</sup>Hg<sup>m,g</sup> and <sup>197</sup>Hg<sup>m,g</sup> to evaluate the experimental cross section data, *Phys. Rev. C* **85**, 034605 (2012).
- [20] J. F. Ziegler, M. D. Ziegler, and J. P. Biersack, SRIM - The stopping and range of ions in matter, *Nucl. Instrum. Methods Phys. Res. B* **268**, 1818 (2010).
- [21] Genie 2000 basic spectroscopy software, version 3.2, [www.Canberra.com](http://www.Canberra.com)
- [22] K. R. Kim, Y. S. Cho, H. J. Kim, J. H. So, and M. Y. Lee, Proton energy measurement using Si(Li) and scintillation crystal detector in the MC-50 cyclotron, *J. Nucl. Sci. Technol.* **45**, Suppl. 5, 538 (2008).
- [23] A. Ferrari, P. R. Sala, A. Fassò, and J. Ranft, "FLUKA: a multi-particle transport code", CERN 2005-10, INFN/TC\_05/11, SLAC-R-773, 2005, <http://www.fluka.org/fluka.php?id=fqa&sub=13>.
- [24] L. Mokhtari Oranj, N. S. Jung, J. H. Oh, and H. S. Lee, 100-MeV proton beam intensity measurement by Au activation analysis using <sup>197</sup>Au(p, pn)<sup>196</sup>Au and <sup>197</sup>Au(p, p3n)<sup>194</sup>Au reactions, *Nucl. Instrum. Methods Phys. Res. B* **375**, 26 (2016).
- [25] R. Michel, R. Bodemann, H. Busemann, R. Daunke, M. Gloris, H. J. Lange, B. Klug, A. Krins, I. Leya, M. Luepke, S. Neumann, H. Reinhardt, M. Schnatz-Buettgen, U. Herpers, T. Schiek, F. Sudbrock, B. Holmqvist, H. Conde, P. Malmborg, M. Suter, B. Dittrich-Hannen, P. W. Kubik, H. A. Sinal, and D. Filges, Cross sections for the production of residual nuclides by low- and medium-energy protons from the target elements C, N, Mg, Al, Si, Ca, Ti, V, Mn, Fe, Co, Ni, Cu, Sr, Y, Zr, Nb, Ba and Au, *Nucl. Instrum. Methods Phys. Res. B* **129**, 153 (1997).
- [26] C. L. Dunford and T.W. Burrows, Online Nuclear Data Service, Report IAEA-NDS-150 (NNDC Informal Report NNDC/ONL-95/10), Rev. 95/10, International Atomic Energy Agency, Vienna, Austria, 1995.
- [27] A. J. Koning and J. P. Delaroche, Local and global nucleon optical models from 1 keV to 200 MeV, *Nucl. Phys. A* **713**, 231 (2003).
- [28] W. Hauser and H. Feshbach, The Inelastic Scattering of Neutrons, *Phys. Rev.* **87**, 366 (1952).
- [29] A. Gilbert and A. G. W. Cameron, A composite nuclear-level density formula with shell corrections, *Can. J. Phys.* **43**, 1446 (1965).
- [30] W. Dilg, W. Schantl, H. Vonach, and M. Uhl, Level density parameters for the back-shifted Fermi gas model in the mass range  $40 < A < 250$ , *Nucl. Phys. A* **217**, 269 (1973).
- [31] L. Kopecky and M. Uhl, Test of gamma-ray strength functions in nuclear reaction model calculations, *Phys. Rev. C* **41**, 1941 (1990).

- [32] A. Spyrou, A. Lagoyannis, P. Demetriou, and S. Harissopoulos, Cross section measurements of ( $p, \gamma$ ) reactions on Pd isotopes relevant to the  $p$  process, *Phys. Rev. C* **77**, 065801 (2008).
- [33] S. Harissopoulos, A. Spyrou, V. Foteinou, M. Axiotis, and G. Provatas, Systematic study of proton capture reactions in medium-mass nuclei relevant to the  $p$  process: The case of  $^{103}\text{Rh}$  and  $^{113,115}\text{In}$ , *Phys. Rev. C* **93**, 025804 (2016).
- [34] E. Bauge, J. P. Delaroche, and M. Girod, Lane-consistent, semimicroscopic nucleon-nucleus optical model, *Phys. Rev. C* **63**, 024607 (2001).
- [35] S. Watanabe, High energy scattering of deuterons by complex nuclei, *Nucl. Phys.* **8**, 484 (1958).
- [36] L. McFadden and G. R. Satchler, Optical-model analysis of the scattering of 24.7 MeV alpha particles, *Nucl. Phys.* **84**, 177 (1966).
- [37] P. Demetriou, C. Gramma, and S. Goriely, Improved global  $\alpha$ -optical model potentials at low energies, *Nucl. Phys. A* **707**, 253 (2002).
- [38] V. Avrigeanu, M. Avrigeanu, and C. Manailescu, Further explorations of the  $\alpha$ -particle optical model potential at low energies for the mass range  $A \approx 45\text{--}209$ , *Phys. Rev. C* **90**, 044612 (2014).
- [39] M. Nolte, H. Machner, and J. Bojowald, Global optical potential for  $\alpha$  particles with energies above 80 MeV, *Phys. Rev. C* **36**, 1312 (1987).
- [40] V. Avrigeanu and P. E. Hodgson, Global optical potentials for emitted alpha particles, *Phys. Rev. C* **49**, 2136 (1994).
- [41] A. V. Ignatyuk, J. L. Weil, S. Raman, and S. Kahane, Density of discrete levels in  $^{116}\text{Sn}$ , *Phys. Rev. C* **47**, 1504 (1993).
- [42] S. Goriely, F. Tondeur, and J. M. Pearson, A Hartree-Fock nuclear mass table, *At. Data Nucl. Data Tables* **77**, 311 (2001).
- [43] S. Goriely, S. Hilaire, and A. J. Koning, Improved microscopic nuclear level densities within the HFB plus combinatorial method, *Phys. Rev. C* **78**, 064307 (2008).
- [44] S. Hilaire, M. Girod, S. Goriely, and A. J. Koning, Temperature dependent combinatorial level densities with the D1M Gogny force, *Phys. Rev. C* **86**, 064317 (2012).
- [45] D. M. Brink, Individual particle and collective aspects of the nuclear photo effect, *Nucl. Phys.* **4**, 215 (1957).
- [46] P. Axel, Electric dipole ground-state transition width strength function and 7-Mev photon interactions, *Phys. Rev.* **126**, 671 (1962).
- [47] E. Khan, S. Goriely, D. Allard, E. Parizot, T. Suomijarvi, A. J. Koning, S. Hilaire, and M. C. Duijvestijn, Photodisintegration of ultra-high-energy cosmic rays revisited, *Astropart. Phys.* **23**, 191 (2005).
- [48] S. Goriely, Radiative neutron captures by neutron-rich nuclei and the r-process nucleosynthesis, *Phys. Lett. B* **436**, 10 (1998).